Design and Simulation of Liquid Krypton as Gamma Ray Detector

Syed M. Hassan, Ahmed Hassanein, David S. Koltick, Nader Satvat, and Xue Yang

***Abstract*—Monte Carlo simulations were used to model gamma ray interactions at 1 MeV and 11 MeV within liquid krypton to understand geometry effects and energy containment. Two Monte Carlo codes were used in this work: Geant4 and MCNP5. The agreement of the two codes was shown by the comparison of the calculated average energy deposition and fraction of incident gamma energy deposited as a function of chamber lengths and gamma ray offsets. Modeling shows that good energy containment for 1 MeV gamma rays occurs for chamber depths of 20 cm. For gamma rays entering parallel to the central axis of the detector, 1 MeV showers are well contained up to approximately 1 cm of the detectors' edge. For 11 MeV gamma rays the acceptance plateau occurs at a depth of 40 cm and 20 cm from the detectors' edge.**

***Index Terms*—Gamma ray detector, Geant4, liquid krypton, liquid noble gas, MCNP5, Monte Carlo simulation.**

I. Introduction

NUCLEAR waste will continue to be stored at a large and increasing number of sites above the ground for at least the next 50 years. Safeguard measures will require better knowledge of the exact elemental content of this rapidly growing material inventory [1], [2]. In addition, spent fuel assay of fuel bundle assemblies is a difficult task due to high gamma radiation fields with the attendant dead tines and radiation damage when using present technology gamma ray crystal detectors, NaI(Tl) or solid-state HPGe detectors [3], [4]. Therefore, the ultimate goal of this project is to extend the present Liquid Noble Gas (LNG) detector technology from the low rate, low radiation background environments as has been used for astrophysical dark matter searches [5], to the high rate, high radiation environment found near spent fuel assemblies [6].

We present simulation results for liquid krypton motivated by the lower cost of krypton compared to xenon, yet having similar stopping power. The specific aims are to understand the necessary physics processes of radiation interactions and geometry effects for gamma ray detectors as a function of depth and gamma ray offset relative to the central axis of the cylindrical detector.

Manuscript received September 18, 2012; revised December 15, 2012; accepted February 08, 2013. Date of current version April 10, 2013. This work was supported in part by the U.S. Domestic Nuclear Detection Office (DNDO) and National Science Foundation (NSF) under grant 1140026.

S. M. Hassan, X. Yang, N. Satvat, and A. Hassanein are with the School of Nuclear Engineering, Purdue University, West Lafayette, IN 47907 USA (e-mail: smhassan@purdue.edu).

D. S. Koltick is with the Department of Physics, Purdue University, West Lafayette, IN 47907 USA (e-mail: koltick@purdue.edu).

Color versions of one or more of the figures in this paper are available online at http://ieeexplore.ieee.org.

Digital Object Identifier 10.1109/TNS.2013.2252195

II. Physics Models

Geant4 [7] and MCNP5 [8] are libraries of code for the simulation of the passage of particles through matter. All aspects of these codes are at the control of the developer, especially the physics processes chosen to be included. The developer weighs the included details against CPU performance. We use these codes for LNG detector design focused on gamma ray detection over the range 200 keV to 11 MeV for elemental analysis using nuclear gamma emission. This energy range falls into the Geant4 low energy electromagnetic (EM) physics model and is well suited for calculations by MCNP5.

A. Geant4

In simulations using Geant4, the Livermore low-energy electromagnetic models were chosen as the primary EM physics processes. The model makes direct use of atomic shell cross section data for standard processes. Parameterizations of these data have been made to optimize the code for high-energy physics applications [9]. The simulation includes Rayleigh scattering, photoelectric effect, Compton scattering and gamma conversion for gamma reactions; multiple scattering, ionization, bremsstrahlung, annihilation for electron and positron reactions. Future simulations will include both Cerenkov and scintillation processes for the creation of the optical photons important to understanding the energy resolution of the detector. The cross sections are extracted from Evaluated Photons Data Library (EPDL97) [10], Evaluated Electron Data Library (EEDL) [11], Evaluated Atomic Data Library (EADL) [12] and binding energy values based on data of Scofield [13]. The cut-off energies for all particles are set to 250 eV that is the low energy applicability limit of the Livermore low-energy EM models.

B. MCNP5

MCNP [8] is a general purpose Monte Carlo N-particle code that models the transport of coupled neutron, photon and electron interactions. The MCNP5 photon interactions include photoelectric effect, incoherent and coherent scattering, fluorescent emission and pair production whose cross sections are based on ENDF/B-VI.8 [14] and EPDL97 libraries. The electron and positron processes in MCNP5 account for angular deflection through multiple Coulomb scattering, collisional energy loss with optional straggling, ionization, bremsstrahlung, and annihilation. The electron-positron processes also rely on experimental data based libraries.

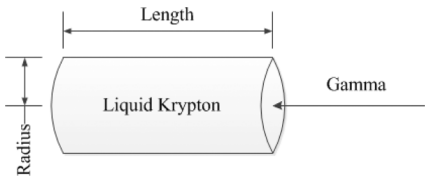

Fig. 1. Geometry of the liquid noble gas detector.

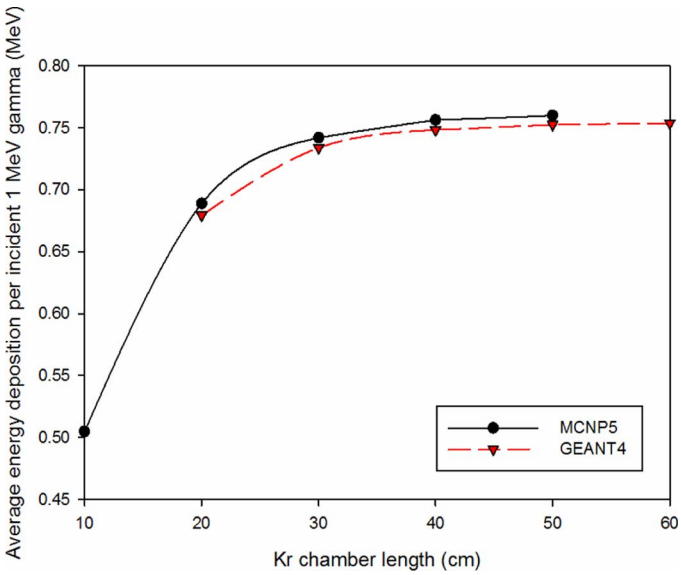

Fig. 2. Average energy deposition per incident 1 MeV gamma at a fixed chamber radius of 5 cm. Data points are fit by a polynomial cubic spline (solid and dashed lines).

III. Results for 1 MeV Gamma Rays

A. Effect of Chamber Length

The detector geometry is a simple cylinder filled with liquid Kr (LKr) as shown in Fig. 1. Two energies at the extremes of the energy range of interest were simulated in detail: 1 MeV and 11 MeV. A monochromatic beam parallel to the axis of the cylinder was placed at the center of the LKr chamber. The beam radius was set to a line beam and the LKr chamber radius was set to 5 cm for the case of 1 MeV gamma rays. The average energy deposition per incident gamma was calculated using both Geant4 and MCNP5 for various chamber lengths. The statistical uncertainties were insignificant to be indicated in the figures.

Fig. 2 shows the simulated average energy deposition per incident 1 MeV gamma for various LKr chamber lengths. The data points are plotted without the error bars for clearness. The Geant4 and MCNP5 results agree well with a difference of only $\sim 1\%$ due to different data libraries. The curves start saturating at 25 cm. Therefore, a chamber length greater than 20 cm is enough to collect most of the energy of the 1 MeV gamma rays.

B. Effect of Beam Offset

Similar simulations for 1 MeV gamma rays were performed as a function of beam offset. The beam offset is defined as the distance between the location of the beam and the center of the cylinder axis. In these simulations, the chamber radius and length were fixed at 5 and 20 cm, respectively. Fig. 3 presents the average energy deposition per incident 1 MeV gamma as a function of beam offset. Spline functions are used to fit the data points. The Geant4 and MCNP5 also agree well with a difference of $\sim 1\%$. Moving the beam from the center to the 4 cm offset location does not significantly change the average energy deposition into the LKr chamber. This indicates that the 1 MeV incident gamma deposits most of its energy along the cylinder axis.

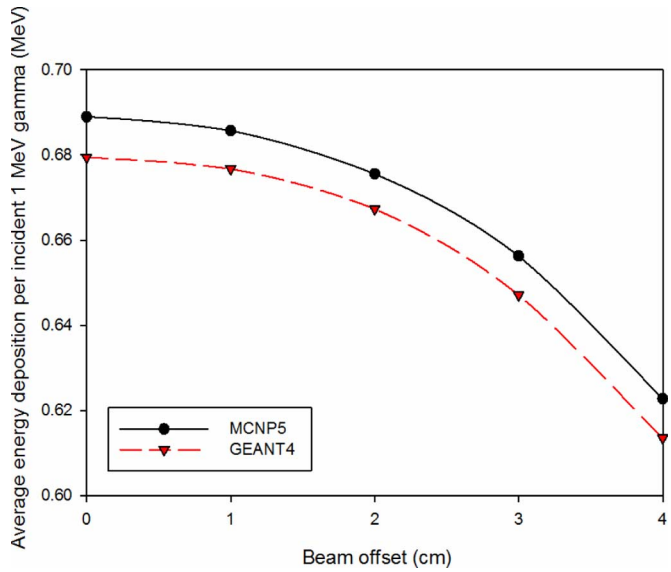

Fig. 3. Average energy deposition per incident 1 MeV gamma for beam offset of 0–4 cm. LKr chamber radius and length are 5 and 20 cm, respectively.

TABLE I
Average and Maximum Number of Physics Processes

		1 MeV	11 MeV
γ	Rayleigh	0.273 (6) [a]	1.09 (26)
	Photoelectric	2.68 (12)	18.6 (44)
	Compton	3.33 (13)	8.41 (38)
	Gamma conversion	0 (0)	0.739 (3)
$E_{deposit}$	All (MeV)	0.974 (97.4%) [b]	10.5 (95.5%)
	γ (MeV)	0.0120 (1.23%) [c]	0.0559 (0.532%)
	e- (MeV)	0.962 (98.8%)	9.38 (89.3%)
	e+ (MeV)	0 (0%)	1.11 (10.6%)

[a]The average number of reactions triggered by an incident gamma. Numbers in bracket are the maximum number of reactions introduced.

[b]The average energy deposition per incident gamma. Numbers in bracket are the percentage of deposited energy with respect to the incident gamma energy.

[c]The average energy deposition per incident gamma by certain type of particle. Numbers in bracket are the percentage of deposited energy by certain type of particle with respect to the average total energy deposition.

C. Photopeak Efficiency

The simulations also yield the fraction of incident gammas that deposit at least certain amount of energy in the LKr chamber. These studies yield information on the photopeak efficiency. Fig. 4(a) illustrates the fraction of energy deposition as a function of length for incident gammas that deposit more than 50%, 60%, and up to 90% energy into the LKr volume calculated by Geant4. It was found that the fractional

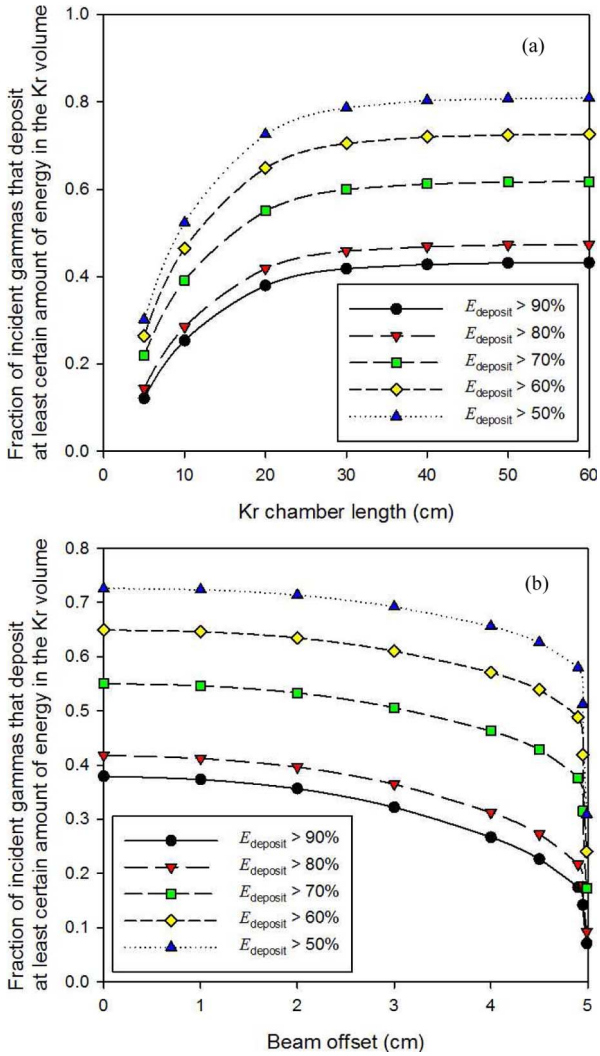

Fig. 4. Fractional energy deposition for 1 MeV gammas in the LKr chamber simulated by Geant4: (a) LKr chamber radius fixed at 5 cm. (b) LKr chamber radius fixed at 5 cm and length fixed at 20 cm. (E_{deposit} denotes the energy deposited in LKr volume and data points are fit by the polynomial cubic spline).

acceptance changes little for fractions above 90%. The curve shapes are similar to Fig. 2. Beyond chamber lengths of 20 cm, the photopeak efficiency is about 40% for 1 MeV gamma ray incident on the cylinder's central axis. Fig. 4(b) depicts the same fractions as a function of beam offsets, for the case of a chamber with 5 cm radius and 20 cm length. In Fig. 4(b), the calculation of beam offsets includes values at 4.5, 4.9, 4.95 and 4.99 cm. The curves rapidly decrease when the beam was placed about 0.5 cm from the edge.

The results of $E_{\mathrm{deposit}} > 90\%$ in both Fig. 4(a) and (b) were also calculated by MCNP5. All absolute differences between MCNP5 and Geant4 are smaller than 1%.

IV. Results for 11 MeV Incident Gammas

The extreme energy for elemental analysis occurs at about 11 MeV gamma rays. We investigate the size of LKr volume required for stopping the 11 MeV gammas. Two sets of simulations were carried out using Geant4. One is the simulation of a fixed chamber radius of 30 cm with different chamber lengths; the other is simulated with a fixed chamber length of 60 cm

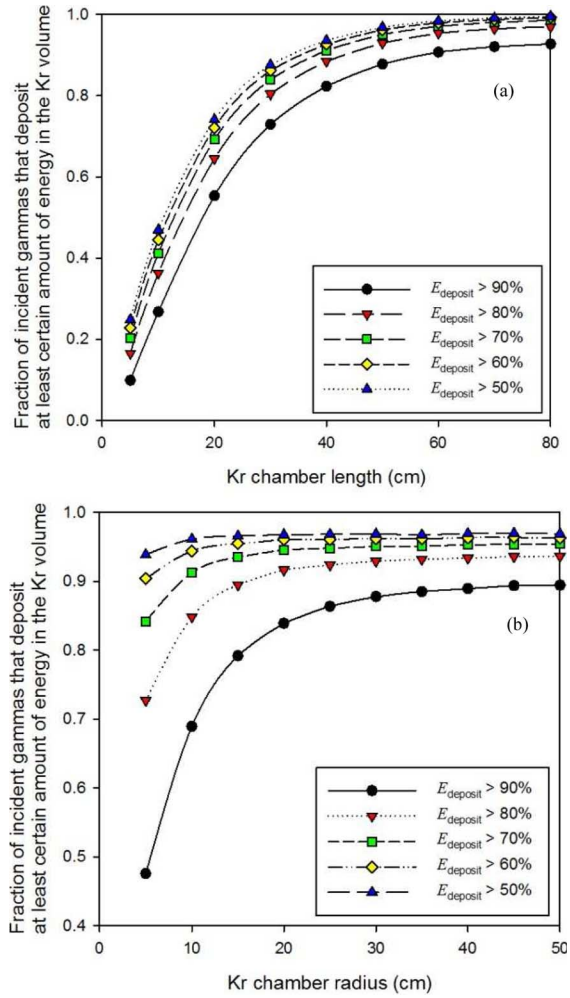

Fig. 5. Fractional energy deposition for 11 MeV gammas in the LKr chamber simulated by Geant4: (a) LKr chamber radius fixed at 30 cm. (b) LKr chamber length fixed at 60 cm.

with different chamber radii. Unlike the 1 MeV simulations, positrons will be created in the LKr volume through pair production in these simulations.

Fig. 5(a) is the fractional energy deposition as a function of chamber length. From the figure the fractional energy deposition has a plateau at about 40 cm, which is about twice the 1 MeV plateau value. Again, the fractional energy acceptance for fractions above 90% are very similar. Photopeak efficiency for on-axis gamma rays for this large chamber volume is nearly 100%.

Fig. 5(b) shows the acceptance as a function of chamber radius at a fixed depth of 60 cm. Chambers with radii of 15–20 cm will produce high photopeak efficiency.

V. Physics Reactions

Table I lists the average and maximum recorded number for each type of physics reactions and the average energy deposition by particle type for both the 1 MeV and 11 MeV simulations. In both the 1 and 11 MeV cases, the LKr chamber radius and length are 30 and 60 cm, respectively, and the results are based on 0.1 M particles per simulation. In all simulations the gamma rays were directed along the central axis of the cylinder.

VI. Conclusions

Two Monte Carlo codes, Geant4 and MCNP5, were used for the development of a liquid krypton gamma-ray detector. The agreement of the two codes was shown by the results of the energy deposition of 1 MeV and 11 MeV gamma rays for different LKr cylinder chamber lengths and beam offsets to be within 1%. Future simulations will include all the necessary scintillation processes for the creation of the optical photons important to understanding the energy resolution of the detector.

References

[1] Special Nuclear Material, U.S. Nuclear Regulatory Commission. [Online]. Available: www.nrc.gov/materials/sp-nucmaterials.html, accessed Mar. 2010

[2] R. C. Runkle, L. E. Smith, and A. J. Peurrung, "The photon haystack and emerging radiation detection technology," *J. Appl. Phys.*, vol. 106, p. 041101, 2009.

[3] B. Ayaz-Maierhafer and T. A. DeVol, "Determination of absolute detection efficiencies for detectors of interest in homeland security," *Nucl. Instrum. Methods Phys. Res. A*, vol. 579, p. 410, 2007.

[4] E. R. Siciliano, J. H. Ely, R. T. Kouzes, B. D. Milbrath, J. E. Schweppe, and D. C. Stromswold, "Comparison of PVT and NaI(Tl) scintillators for vehicle portal monitor applications," *Nucl. Instrum. Methods Phys. Res. A*, vol. 550, p. 647, 2005.

[5] E. Aprile *et al.*, "The XENON100 Dark Matter Experiment," *Astroparticle Physics*, vol. 35, p. 573, 2012.

[6] D. S. Koltick and S. Z. Kane, "A cargo inspection system for special nuclear material (SNM) based on associated particle neutron generators and liquid-Kr detectors," in *AIP Conf. Proc.*, 2009, vol. 1099, p. 685.

[7] Geant4 User's Guide for Application Developers. Geant4 collaboration, Version: geant4 9.5, Dec. 2, 2011.

[8] MCNP—A General Monte Carlo N-Particle Transport Code, Version 5, Los Alamos National Laboratory, LA-UR-03-1987, Apr. 24, 2003.

[9] Physics Reference Manual, Geant4 collaboration, Version: geant4 9.5.0, Dec. 2, 2011.

[10] D. Cullen, J. H. Hubbell, and L. Kissel, "EPDL97: The Evaluated Photon Data Library, '97 version," UCRL-50400, vol. 6, rev. 5, 1997.

[11] S. T. Perkins, D. E. Cullen, and S. M. Seltzer, "Tables and Graphs of Electron-Interaction Cross-Sections From 10 eV to 100 GeV Derived From the LLNL Evaluated Electron Data Library (EEDL), Z=1-100," UCRL-50400, vol. 31.

[12] S. T. Perkins, D. E. Cullen, M. H. Chen, J. H. Hubbell, J. Rathkopf, and J. Scofield, "Tables and Graphs of Atomic Subshell and Relaxation Data Derived From the LLNL Evaluated Atomic Data Library (EADL), Z=1-100," UCRL-50400, vol. 30.

[13] J. H. Scofield, "Radiative transitions," in *Atomic Inner-Shell Processes*, B. Crasemann, Ed. New York, NY, USA: Academic Press, 1975, pp. 265–292.

[14] *ENDF-201, ENDF/B-VI Summary Documentation*, P. F. Rose, Ed. Upton, NY, USA: Brookhaven National Lab., Oct. 1991.